The effect of photomask resolution on separation efficiency on microfabricated devices

Amanda R. Meyer, Anna M. Clark and Christopher T. Culbertson*

Received 4th April 2006, Accepted 13th July 2006
First published as an Advance Article on the web 14th August 2006
DOI: 10.1039/b604840d

Separation quality on glass microfluidic devices fabricated from photomasks of different optical resolutions was compared by measuring the dispersion (apparent diffusion) coefficients of a set of standard compounds separated on these devices. Currently, the channel manifolds of most microfluidic devices are patterned using chrome photomasks. A much cheaper, more robust alternative to chrome photomasks are laser photoplotted masks. The primary disadvantage to using laser photoplots is that the optical resolution of these masks is not as high as that of chrome masks, and this feature increases the side-wall roughness of etched channel manifolds patterned using such masks. The increased wall roughness may affect the fluid flow within the channels and, therefore, the separation quality. To determine the effect of increased sidewall channel roughness, microchip channel manifolds were patterned in soda lime glass using a chrome photomask and laser photoplots printed at resolutions of 620, 1240, 3100 and 6200 dots per centimetre (dpc). Separations were performed on these devices using dilute solutions of fluorescently labeled amino acids. The peak variances of the amino acids were calculated at increasing distances down the separation channel and plotted as a function of migration time. From this plot, dispersion coefficients of the analytes were measured. This allowed for a reliable, relatively easy, direct separation analysis among microchips fabricated from the various photomasks. After multiple separations using microchips fabricated from each resolution mask, we found that the change in sidewall surface roughness did not significantly affect the dispersion coefficients measured, and thus the separation quality. The lower mask resolution limit, rather, was governed by the fidelity to which the mask could capture the original CAD design.

Introduction

In most papers that report the use of microfluidic devices, the channel manifolds, or molds in the case of plastic devices, are fabricated by photolithographic patterning using chrome photomasks. Chrome masks produce smooth channels with nanometre-scale edge roughness. While such masks are commonplace they are expensive, fragile, and the thin layer of chrome is subject to pinholes and scratching. In rapid prototyping applications, several iterations of a design may be necessary to optimize operation. In addition, as more functional elements are integrated into a microfluidic device, the manifold gets increasingly complex and often several redesigns are necessary in order to optimally integrate the components; therefore, more economical options for mask production would be desirable. One option is to use laser photoplots or simple high resolution laser printing on transparencies. At the present time laser printer transparencies are not capable of adequately producing the 20 μm feature sizes that we desire, but laser photoplots are. Laser photoplots are fabricated by layering sub-micron silver halide crystals onto a film of Mylar or similar plastic. Patterns are then written by raster scanning a laser across the light sensitive film to produce an image.[1] The resolution of the mask features is a function of the silver halide grain size, the laser focus spot size, and the stepper motor resolution that controls the laser position. Resolution, generally measured as a plot density in dots per centimetre (dpc), ranges from 620 dpc to >6200 dpc for these masks. The minimum feature sizes for such plots are ~12 to <7 μm, respectively, and the distances between parallel edges of small geometric patterns can be maintained to tolerances within about three times the resolution of the plotter. The edge roughness of the 6200 dpc photoplots is reported to be ~2 μm for both horizontal and vertical features. In general, the minimum feature size decreases and edge definition increases with increasing resolution.

Laser photoplots are 60 to 250 times cheaper than conventional electron beam and flash lamp produced chrome masks depending upon resolution (plot density), as can be seen

Table 1 Cost comparison table of various photomasks

Resolution	Size and cost	Cost per cm^2
620 dpc[a] *1/4th mil*	25.4 × 30.48 cm $14.00	$0.01808
1240 dpc *1/8th mil*	25.4 × 30.48 cm $10.45	$0.01350
3100 dpc *1/20th mil*	25.4 × 30.48 cm $26.22	$0.03387
6200 dpc *1/40th mil*	25.4 × 30.48 cm $65.01	$0.08397
Chrome	12.7 × 12.7 cm $800	$4.9600

[a] The 620 dpc mask was purchased from a different company than the other photoplotted photomasks.

Department of Chemistry, Kansas State University, 111 Willard Hall, Manhattan, KS, 66506, USA. E-mail: culbert@ksu.edu; Fax: +1-785-532-6666; Tel: +1-785-532-6685

in Table 1 below. In addition to being less expensive than chrome photomasks, the photoplots are generally more opaque and have fewer pinhole defects than chrome masks. Because they are printed in a flexible matrix on a flexible substrate, we have also found them to be generally more robust than their chrome counterparts. The major drawback of these masks is the feature sizes that can be reliably printed. For the highest resolution laser photoplots, earlier studies have shown this to be $\sim$7 μm.[1] For most of the applications in our lab, such feature sizes are more than adequate. In fact, laser photoplots have been successfully used to fabricate a variety of micro-scale devices for both microelectromechanical and microfluidics applications.[2] While laser photoplots have been used previously to fabricate microchips,[1,2] no study has been made as to how the increased edge roughness imparted to the channel sidewalls during the patterning process affects separation quality.

Numerous factors can affect separation efficiency on microfluidic devices. Many of these factors in some way involve the channel walls. As microchips fabricated from laser photoplots have channel sidewalls rougher than those fabricated from chrome masks, such roughness may affect the separation quality. Little has been published on the effects of surface roughness on separation quality, but the effects of surface roughness have been described by mathematical modeling.[3] In these studies, increases in surface roughness lead to variations of electroosmotic flow (EOF). Such variations in EOF would generate pressure differentials along the channel and, therefore, some type of parabolic flow profile, as opposed to the flat flow profile generated in channels with constant EOF. Such pressure-induced flows will lead to band broadening beyond that due to molecular (longitudinal) diffusion and, therefore, degrade separation quality.

There are several potential metrics that can be used to assess separation quality. These include the number of plates generated (N), plate height (H), the resolution between two analytes (Rs), and analyte peak height (h). Unfortunately, typical chip-to-chip and run-to-run variation in EOF and temperature can lead to significant variability in the experimentally obtained values that may have nothing to do with the separation channel roughness. In addition, small chip-to-chip changes in channel lengths, the optimal potentials for injection and injection plug length can further complicate the use of such metrics. In order to focus on the basic band broadening mechanisms and avoid some of these other variables, one can measure the dispersion (or apparent diffusion) coefficient of a series of analyte plugs as they travel through the channel. The dispersion coefficient includes the effects of basic longitudinal (or molecular) diffusion and other dynamic random processes that occur during a separation.[4] These random processes generally lead to Gaussian distributions of molecules in analyte bands (peaks), and dispersion coefficients (D_T) can be measured from these peaks using the Einstein–Smoluchowski equation:

$$\sigma_l^2 = 2D_T t \tag{1}$$

where σ_l^2 is the spatial analyte band variance and t is the time over which the dispersion is measured; *i.e.* in our case the analyte migration time. By plotting the peak variance as a function of migration time, where the migration time is varied by changing the detection distance, the dispersion coefficients can be determined.[5] Such measurements are independent of variations in injection plug length, electric field, EOF, analyte mobility and migration time as might be common among a set of microchips. In addition, if the temperature varies among runs, such changes can be corrected based upon the Stokes–Einstein relationship[6] as shown in eqn (2) below:

$$D_{25^\circ C} = D_{X^\circ C}\frac{T_{25^\circ C}\eta_{X^\circ C}}{T_{X^\circ C}\eta_{25^\circ C}} \tag{2}$$

where T is the temperature and η is the viscosity of water at temperature X.

If the band broadening occurring during a separation is truly limited to longitudinal diffusion and if the diffusion coefficient is known, then the ratio of the dispersion coefficient to the diffusion coefficient provides a dimensionless parameter that can be used compare band broadening processes performed under different separation conditions. Unfortunately the diffusion coefficients for most analytes are not precisely known in many cases, so such dimensionless values can not be calculated. Nonetheless simple comparisons of dispersion coefficients still allow for a fundamental comparison of band broadening among separations performed under different conditions where one wants to assess the various dynamic band broadening mechanisms that are occurring during a separation; *e.g.* molecular diffusion, potential pressure induced band broadening, Joule heating, rapid adsorption/desorption phenomena. These are the parameters that one might expect to be affected by channel surface roughness. Finally, the dispersion coefficient is directly related to the peak variance (eqn (1)), and therefore, plays a fundamental role in describing the separation efficiency (N), analyte resolution (Rs), and peak height (h) as shown in eqn (3), (4), and (5):

$$N = \frac{t^2}{\sigma_t^2} \tag{3}$$

$$h = \frac{A}{\sigma_t\sqrt{2\pi}} \tag{4}$$

$$Rs = \frac{t_2 - t_1}{2(\sigma_{t2} + \sigma_{t1})} \tag{5}$$

where σ_t^2 is the temporal variance, σ_t is the temporal standard deviation, and A is the peak area. In all cases, the smaller the dispersion coefficient the better the separation performance.

In this paper we report how the resolution of the photomask used to pattern a microchip manifold affects the separation quality by measuring the dispersion coefficients of FITC-labeled amino acids separated on the microchips.

Materials and methods

Reagents and fluorescent derivatization

Arginine (Arg) and Serine (Ser) were obtained from INC Biomedicals Inc. (Aurora, OH). The α-lactalbumin was obtained from Sigma (St. Louis, MO). Fluorescein isothiocyanate (FITC) was obtained from Molecular Probes (Eugene,

OR). Acetone, methanol, sodium tetraborate, sodium hydroxide and dimethylsulfoxide (DMSO) were obtained from Fisher (Pittsburg, PA). 10 mM stock solutions of the amino acids and a 5 mM stock solution of α-lactalbumin were prepared in 150 mM sodium bicarbonate (pH 9). A 10 mM stock solution of FITC was prepared in DMSO. 100 μL of the FITC stock solution were added to 900 μL of each amino acid stock solution and vortexed for 1 min. The FITC stock solution was also added to the α-lactalbumin stock solution in a 1 : 1 molar ratio. The labeling solutions were then placed in the dark for 4 hrs at room temperature. After 4 h the labeled amino acids were frozen, and the labeled α-lactalbumin was placed in the refrigerator until needed. All labeling and buffer solutions were made using distilled deionized water from a Barnstead Ultrapure Water System (Dubuque, IA) and filtered using 0.45 μm Millex®-LCR syringe driven filter units (Millipore Corporation; Bedford, MA). The labeled amino acids were diluted 1000-fold from the stock solution to a final concentration of ~1.3 μM in a 1 mM sodium tetraborate solution at pH 9.1. The labeled α-lactalbumin was diluted 50-fold from the stock solution in 10 mM sodium tetraborate, pH 9.1.

Microchip design and fabrication

A simple cross channel design was used in all experiments (Fig. 1). Chip designs were drawn in-house using AutoCAD LT 2002 program from Thompson Learning (Albany, NY) and electronically sent to photomask fabricators for translation and fabrication. The 620 dots per centimetre (dpc) laser photoplot was obtained from Garrett Film Services (Grand Prairie, TX). Precision laser photoplots with resolutions of 1240 dpc, 3100 dpc, and 6200 dpc were obtained from The Photoplot Store (Colorado Springs, CO). An electron beam written chrome mask was obtained from Advance Reproductions Corporation (Andover, MA). Microchips were fabricated from 10.16 cm × 10.16 cm × 0.16 cm soda-lime photomask blanks coated with chrome and AZT positive tone photoresist (Telic Co., Santa Monica, CA). The photomask blanks were patterned using the photomasks. The blanks were exposed to UV light for 10 s at a power of 45 μJ cm^{-2} using a flood exposure system (ThermoOriel, Stratford, CT). The exposed plate was then submerged in a stirred solution of Microposit Developer (Shipley Co., Marlborough, MA) for 90 s, followed by a thorough rinse with 18 MΩ cm water. The plate was subsequently submerged in a stirred solution of Chrome Mask Etchant (Transene, Co., Danvers, MA) for 3 minutes, rinsed with 18 MΩ cm water, and dried with inert gas. The exposed glass was wet chemically etched using a stirred, dilute buffered oxide etchant (Transene Co., Danvers, MA). The buffered oxide etchant (NH_4F/HF, 10 : 1) was diluted with water and mixed with HCl in the volumetric proportions 1 : 4 : 2, respectively. The channel dimensions were periodically measured throughout the etching process using a stylus-based surface profiler (Ambios Technology; Santa Cruz, CA). Once the channels were the desired depth, the remaining photoresist was removed by rinsing the plate with acetone, followed by a 18 MΩ cm water rinse. The remaining chrome was then removed by immersing the plate in a stirred solution of Chrome Mask Etchant for 10 min, followed by rinses in 1 M sulfuric acid and 18 MΩ cm water. The cleaned plate was then dried with inert gas, and diced into 8 individual 2.54 cm × 5.08 cm slides using a dicing and cutting saw (Model EC-400, MTI Corp., USA). Access holes were mechanically drilled into 10.16 cm × 10.16 cm × 0.16 cm cover plates (Technical Glass Inc., Aurora, CO), then cut into 8 individual slides in a similar manner prior to bonding.

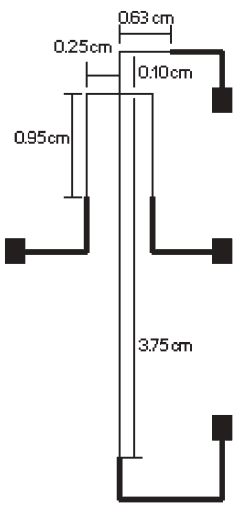

Fig. 1 Schematic of the photomask and the resultant glass chips used for the amino acid separations.

Microchip bonding

The 8 top and bottom slides were cleaned thoroughly by swabbing with acetone followed by rinses with ethanol and 18 MΩ cm water. The chips were then dried with inert gas. Next, the slides were submerged in a stirred 5 M sulfuric acid solution for 5 min, rinsed with 18 MΩ cm water, and then cleaned using the above described acetone–ethanol–water–inert gas procedure. In a laminar flow hood, the slides were immersed in a Versa-Clean Liquid soap solution (Fisher Scientific, Pittsburgh, PA), sonicated (3510 ultrasonic cleaner; Branson, Danbury, CT) for 15 minutes, rinsed with 18 MΩ cm water and dried. The slides were then sonicated in acetone for 10 min, dried, and placed in the previously described dilute buffered oxide etch solution for 10 s. The slides were immediately rinsed with 18 MΩ cm water and placed in a dilute hydrolysis solution (1 : 1 : 2 parts NH_4OH, H_2O_2, H_2O, respectively) for 12 minutes at 60 °C.[7] The slides were then rinsed with 18 MΩ cm water and sonicated in flowing 18 MΩ cm water for 60 s before joining. The etched slides were removed one at a time from the flowing water under a stream of 18 MΩ cm water and placed on a Cleanroom Wiper (DURX 670; Great Barrington, MA). The drilled cover slides were removed from the flowing water and placed on top of the respective etched slide. Binder clips were fastened on the perimeter of the chip to ensure contact between the two surfaces, and water was removed from the channels with a vacuum hose. The joined chips were placed in the oven at 95 °C for 15 min to drive out any remaining water and then annealed

at 565 °C to ensure proper bonding of the cover plate to the chip surface. In the past six months, we have successfully bonded 112 of 112 microchips using this method, for a bonding success rate of 100%. Cylindrical glass reservoirs (~140 μL capacity) were attached using Epo-tek 353ND Epoxy (Epoxy Technologies, Inc., Billerica, MA) where the access holes were located.

Separations and detection

Electrophoretic separations of the FITC-labeled amino acids were performed using a 1 mM sodium tetraborate buffer. FITC-labeled α-lactalbumin separations were performed using a 10 mM sodium tetraborate buffer. Electric potentials for gated injections and separations were applied to the sample, buffer, and sample waste reservoirs using three independent and remotely programmable high-voltage (0–10 kV) power sources from EMCO (Sutter Creek, CA). The samples were injected into the separation channel using 0.02 s gated injections, and the proper potentials were calculated using Kirchhoff's rules and Ohm's law.[8] The timing and magnitude of the electric potentials were controlled by an in-house written LabVIEW program and detected by laser-induced fluorescence (LIF) on a single point setup as previously described in the literature.[9,10]

Scanning electron microscopy

Images of nonbonded, etched microchannels were taken at the injection cross for each type of photomask used. The etched channel manifolds were first cut into one centimetre squares encompassing the cross intersection, and then a 40/60 noble metal mixture of palladium and gold was sputter coated (Desk II Sputter/Etch Unit; Denton Vacuum, LLC; Moorestown, NJ) onto the open-faced microchip to a thickness of 4 nm onto the wafers. SEM images of each chip were taken 40° from normal with a Scanning Electron Microscope (S-3500N, Hitachi Science Systems, Ltd, Ibaraki, Japan) using an Absorbed Electron Detector (S-6542, Hitachi Science Systems, Ltd, Ibaraki, Japan). Images taken at a 40° angle were magnified 800×.

Optical microscopy

The microchips were imaged using a Nikon Eclipse TE2000E microscope with an epiluminescent illumination attachment. Photographs were taken using a 16-bit CCD camera (Princeton Instrument's Micromax, Roper Scientific, Trenton, NJ), and a Sony CCD color video camera (SSC-DC50A). The optical images of the chip intersection were taken with 600× magnification.

Dispersion coefficient measurements

The dispersion coefficient measurements were taken in the center of the separation channel at distances of 1.25 cm, 1.56 cm, 1.88 cm, 2.19 cm, 2.50 cm, and 2.81 cm from the center of the injection cross. Five runs were made at each detection distance on a minimum of three chips fabricated from photomasks at each plot density. The analyte band variance was measured using Igor Pro (WaveMetrics, Inc., Lake Oswego, OR) and plotted as a function of migration time. The dispersion coefficient was then obtained from the slope of the plot. Because the separations were performed on an unthermostatted system, temperature fluctuations were apparent and can cause a 2% per °C change in the measured dispersion coefficient.[5] Therefore, all of the dispersion coefficient measurements taken at temperature X were normalized to 25° using eqn 2 above.

Channel roughness measurements

The edge roughness of the channel wall was measured as a ratio by laying a line down along the edge of the channel on the SEM image and dividing that by the equivalent straight line length. SEM images shown in Fig. 2F–J were enlarged and printed out on a high resolution printer. From the bottom of the injection cross on the print, a linear distance of 9 cm (actual microchip distance of 54.2 μm) was marked along each side of the channel wall. Non-elastic string was then conformed along the top of each side of the channel wall image for the 9 cm linear distance. The string was then removed, measured, and the average length determined. This

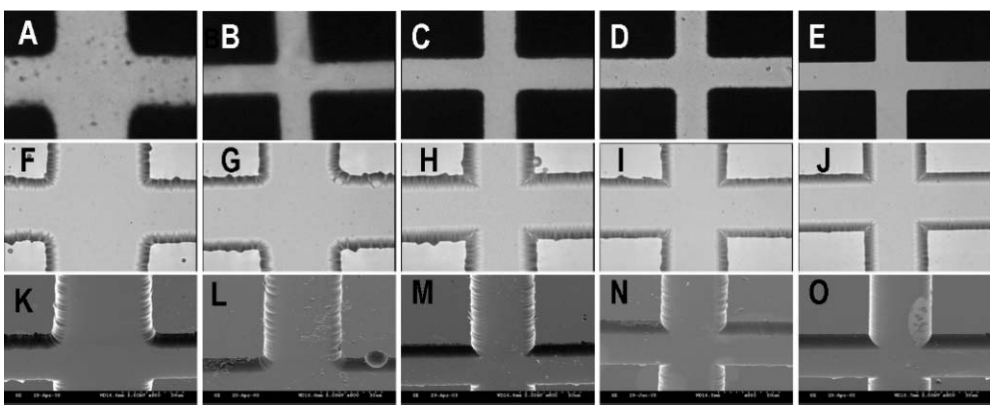

Fig. 2 Optical microscope images taken at 600× of the injection cross from photomasks (A) 620 dpc photoplot (B) 1240 dpc photoplot (C) 3100 dpc photoplot (D) 6200 dpc photoplot (E) chrome photomask. Optical microscope images of cross from bonded chips at 600× for (F) 620 dpc microchip (G) 1240 dpc microchip (H) 3100 dpc microchip (I) 6200 dpc microchip (J) chrome microchip. SEM Images of the non-bonded injection cross 40° from normal (K) 620 dpc chip (L) 1240 dpc chip (M) 3100 dpc chip (N) 6200 dpc chip and (O) chrome chip.

average length was then divided by the linear constant distance of 9 cm.

Data analysis

In order to compare the dispersion coefficients obtained across the chips made from the different photoplots, a one-way analysis of variance (ANOVA) with Tukey multiple-comparison tests was used (SAS software, SAS Institute Inc., Cary, NC). A probability level of $p < 0.05$ was used to determine whether the dispersion coefficients obtained on the different chips were significantly different from one another.

Results and discussion

Mask cost

The cost per square centimetre for each laser photoplot was calculated based on the fabrication expense for a 25.4 cm × 30.48 cm sheet. These are generally the smallest and most expensive photoplots available. The cost per square centimetre for the chrome photomask was calculated based on the cost of a standard 12.7 cm × 12.7 cm mask. These costs do not include any added fees one might incur for data processing tasks or file formatting. Such costs, however, would be similar for both laser and electron beam/flash lamp written masks. The cost per cm^2 for the photoplotted photomasks are 60 to 250 times less expensive than that of the chrome photomask depending upon the desired resolution as can be seen in Table 1.

Optical comparison of mask resolution

The differences in laser photoplot resolution can be observed easily using optical microscopy. Fig. 2A–E shows the injection crosses of several different resolution laser photoplots and a chrome photomask magnified at 600×. The channel widths in all the patterns are nominally 25 μm. The chrome mask is of considerably superior quality with square corners, no measurable fluctuations in channel width, and no residue left in the channel area. These features begin to degrade as one moves to the laser photoplots and then down in resolution. The 620 dpc photoplot has pronounced rounded corners, variable channel widths, and significant silver halide residue throughout the channel pattern.

The photomasks in Fig. 2A–E were employed to pattern the channels onto the photoresist of the glass microchip substrates. The photoresist on the glass substrates were subsequently developed and channels were etched in the glass, as described in the Material and Methods section above. Both optical and SEM images of the etched channels were obtained. As can be seen in Fig. 2F–O, the photomask edge roughness was transferred to the etched glass chips. Qualitatively, the roughness of the glass sidewalls increased as the mask resolution (plot density) decreased. To try to get a more quantitative measure of the roughness introduced by the masking and patterning process, the length of the sidewall edge was measured from the SEM images of the channels as described in the Material and Methods section. The results can be seen in Table 2, along with the average channel dimensions. While there is a measurable increase in surface roughness when moving from chips patterned using the chrome masks to chips patterned using the laser photoplots, the resolution of the photoplot used seemed to have little effect on the actual edge roughness. This is probably due to the fact that we were only able to measure a single line along the top edge of the sidewall. Unfortunately, because of the angle of the sidewall, we could not apply other methods such as AFM or stylus based profilers that are usually used to quantitate surface roughness. The sidewall roughness and the silver halide residue seen on the lower resolution photoplots did not measurably affect the roughness on the channel bottoms. Infrequently, however, some of the etched channels were also very rough on the bottom (Fig. 3). Such roughly etched chips occurred over a range of mask resolutions and under a variety of etching conditions indicating that the roughness was due to some intrinsic factor in the glass rather than the channel patterning step. Nonetheless, all of the microchips fabricated filled with fluid easily and the wall roughness did not lead to bubble nucleation and generation.

Effects of mask resolution on separation quality

In order to determine the effects of the channel sidewall roughness on separation quality, electrophoretic separations of FITC-labeled Arg and Ser were performed, and the separated analytes were detected at several distances from the injection point. Plots of analyte band variance *vs.* migration time were made and the dispersion coefficients were measured from the slope of these plots as described in the Material and Methods Section. A typical plot is shown in Fig. 4. Dispersion coefficients were measured on at least three chips patterned from each type of photomask, and the results are shown in

Table 2 Channel surface roughness measurements and dimensions. Roughness measurements were calculated from the corresponding SEM images captured at 40° from normal. Channel dimensions were measured from the channel profiles

Resolution	Side wall roughness[a]	Average injection plug length/cm[b]	Average channel width/μm	Average channel depth/μm	Channel ratio (width/depth)
Chrome	1.0000	1.67×10^{-2}	48.85	11.63	4.21
6200 dpc	1.0500	1.66×10^{-2}	51.96	10.81	4.81
3100 dpc	1.1056	1.45×10^{-2}	53.56	10.98	4.88
1240 dpc	1.0428	1.61×10^{-2}	72.83	10.39	7.01
620 dpc	1.0706	1.41×10^{-2}	80.06	11.52	6.95
Rough Chrome	1.0567	N/A	45.66	10.69	4.27
Rough 3100 dpc	1.1706	1.40×10^{-2}	53.05	11.82	4.49

[a] These numbers represent a relative measure of the roughness of the side channels as explained in the Materials and Methods section. [b] These numbers represent the injection plug length as explained in the Materials and Methods section.

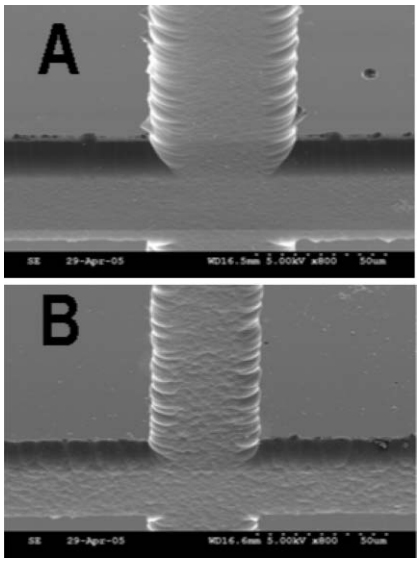

Fig. 3 SEM images taken 40° from normal of a non-bonded injection cross of roughly etched microchannels for (A) 3100 dpc photomask and (B) chrome photomask.

Fig. 5A and B. In order to determine whether there was a statistically significant difference in the dispersion coefficients measured from the different chips a one-way ANOVA was performed on the data. The probability levels (p) for the FITC-arg and FITC-ser dispersion coefficients were 0.1170 and 0.0910, respectively. Because $p > 0.05$, no significant difference exists in the experimentally determined dispersion coefficients for the chips fabricated from the different photomask resolutions. The average dispersion coefficient values for each set of chips were also within experimental error of previously published diffusion coefficient values for similarly sized small molecules like fluorescein and Rhodamine B ($4.25 \pm 0.01 \times 10^{-6}$ cm^2 s^{-1} at 25 °C),[5] indicating that the separations were all diffusion limited.

Similar separations were carried out using α-lactalbumin. The dispersion coefficients for α-lactalbumin measured on the lowest resolution photoplot (620 dpc) and chrome devices were 4.9×10^{-6} cm^2 s^{-1} and 4.8×10^{-6} cm^2 s^{-1}, respectively. While these results were within experimental error of one another, they were also both larger than the expected diffusion coefficient for α-lactalbumin. The excess band broadening,

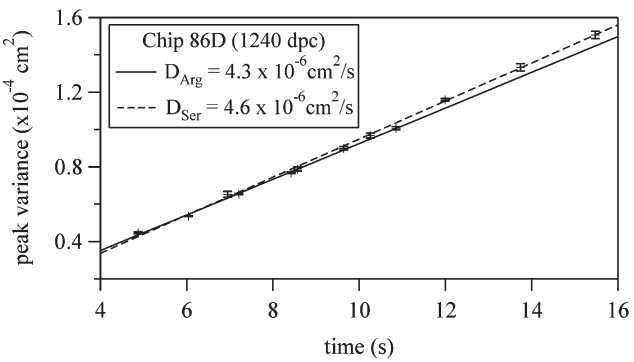

Fig. 4 IGOR graph of peak variance *vs.* migration time with error bars for microchip 86D (1240 dpc).

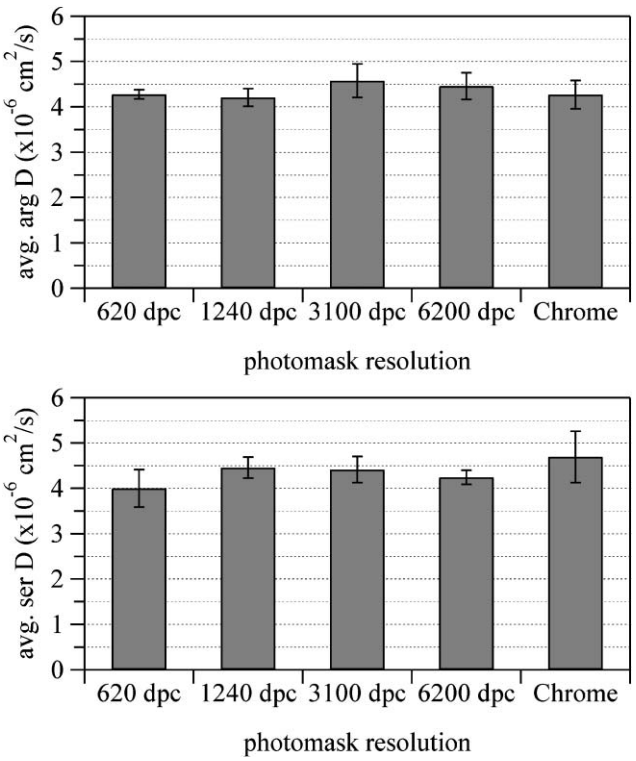

Fig. 5 Average dispersion coefficients of (A) FITC-arginine and (B) FITC-serine. The type of photomask is identified on the x-axis.

however, was not due to the difference in chip side wall roughness as it was of equal magnitude on both devices. Rather, it was probably due to some surface adsorption/desorption phenomena.

Finally, the y-intercept of the variance *vs.* migration time plot (Fig. 4) is a measure of the injection width (σ_{inj}^2) and detection window length (σ_{det}^2) contributions to the overall peak variance as shown by eqn (6):

$$\sigma_{y-int}^2 = \frac{w_{inj}^2}{12} + \frac{w_{det}^2}{12} \quad (6)$$

where w_{inj} is the injection plug length and w_{det} is the width of the detection window. The detection window length can be calculated from the spatial filter size divided by the magnification ($\sigma_{det}^2 = 0.0025$ cm^2 in our case). This allows one to determine the injection plug length from the y-intercept on the graph.[11] As can be seen in Table 2 the average injection width among the 5 different chips patterned from different resolution photoplots are within a very small range and within experimental error of one another. This demonstrates that even the poor cross shapes of the lower resolution chips are still capable of generating small injection plugs.

The results for FITC and α-lactalbumin indicate that there is no correlation between the measured dispersion coefficients and increased channel roughness imparted by patterning chips with laser photoplots. Earlier results from PDMS devices cast from molds patterned with a 1 240 dpc laser photoplot also resulted in diffusion limited separations for a variety of analytes.[10] Other reports of microfluidic devices fabricated using laser photoplots have also yielded good separations

and fluid transport capabilities.[10,12–16] One reason that the increased surface roughness imparted to the channels may not have impacted the separation quality is that the roughness is limited to the sidewalls of the channel. These sidewalls make up <2/9 of the total surface area of the channel. We also, however, tested the microchips which roughly etched on the bottom of the channel. Approximately ½ of the channel surface on these chips were significantly rough, *i.e.* >500 nm rms, as can be seen in Fig. 3A and B. The dispersion coefficients measured for the analytes on these microchips were also within experimental error of the dispersion coefficient measured on the chrome patterned chip. Based on this result it appears that analyte band dispersion, and therefore separation quality, is not adversely affected by increased surface roughness up to at least 500 nm rms.

In terms of the fabrication of microfluidic devices, the real limitation to how low of a resolution laser photoplot that one can use is the fidelity of the mask to the desired channel manifold design. A high resolution photomask is needed if the pattern details are pertinent to the experiment or when the features are small. These results do not at this time correlate well with some theoretical models of the effect of surface roughness on separation quality.[3] Further research is needed to bring the experimental and theoretical results in line with one another.

Finally, because the excitation and emission light enter and exit primarily through the smooth top and bottom of the channel (rather than through the side wall), no degradation in optical properties was seen among the different resolution chips tested above.

Conclusions

Based on experimental data reported above, microfluidic devices patterned using laser photoplots are able to produce separation quality equivalent to microchips patterned using chrome photomasks. For fabrication of microstructures greater than ~10 μm, photoplotted photomasks offer numerous advantages such as significantly lower cost and increased durability.

Acknowledgements

This work was supported by an NSF CAREER award. The authors would like to thank Alan Hartung in the Kansas State University Statistics Lab for assistance in performing the statistical analysis.

References

1 V. Linder, H. Wu, X. Jiang and G. M. Whitesides, *Anal. Chem.*, 2003, **75**, 2522–2527.
2 T. Deng, H. Wu, S. T. Brittain and G. M. Whitesides, *Anal. Chem.*, 2000, **72**, 3176–3180.
3 Y. Hu, C. Werner and D. Li, *Anal. Chem.*, 2003, **75**, 5747–5758.
4 J. C. Giddings, *Unified Separation Science*, John Wiley and Sons, New York, 1991.
5 C. T. Culbertson, S. C. Jacobson and J. Michael Ramsey, *Talanta*, 2002, **56**, 365–373.
6 P. W. Atkins, *Physical Chemistry*, W. H. Freeman and Company, New York, 3rd edn, 1986.
7 S. C. Jacobson, R. Hergenroder, L. B. Koutny, R. J. Warmack and J. M. Ramsey, *Anal. Chem.*, 1994, **66**, 1107–1113.
8 K. Seiler, Z. H. Fan, K. Fluri and D. J. Harrison, *Anal. Chem.*, 1994, **66**, 3485–3491.
9 S. C. Jacobson and J. M. Ramsey, *Anal. Chem.*, 1996, **68**, 720–723.
10 G. T. Roman, T. Hlaus, K. J. Bass, T. G. Seelhammer and C. T. Culbertson, *Anal. Chem.*, 2005, **77**, 1414–1422.
11 D. N. Heiger, *High Performance Capillary Electrophoresis – An Introduction*, Hewlett-Packard Company, France, 2nd edn, 1992.
12 A. K. Price, D. J. Fischer, R. S. Martin and D. M. Spence, *Anal. Chem.*, 2004, **76**, 4849–4855.
13 M. L. Kovarik, M. W. Li and R. S. Martin, *Electrophoresis*, 2005, **26**, 202–210.
14 E. P. Kartalov and S. R. Quake, *Nucleic Acids Res.*, 2004, **32**, 2873–2879.
15 B. H. Huynh, B. A. Fogarty, R. S. Martin and S. M. Lunte, *Anal. Chem.*, 2004, **76**, 6440–6447.
16 C. L. Hansen, M. O. A. Sommer and S. R. Quake, *Proc. Natl. Acad. Sci. U. S. A.*, 2004, **101**, 14431–14436.